Eur. Phys. J. A (2020) 56:22
https://doi.org/10.1140/epja/s10050-020-00029-8

THE EUROPEAN PHYSICAL JOURNAL A

Regular Article - Experimental Physics

Search for proton emission of the isomeric 10^+ state in ^{54}Ni

K. Stahl[1], A. Wendt[1], P. Reiter[1,a], D. Rudolph[2], A. Blazhev[1], B. Bruyneel[1], J. Eberth[1], C. Fahlander[2], C. Fransen[1], P. Golubev[2], H. Hess[1], R. Hoischen[2], A. Holler[1], M. Kalkühler[1], T. Kotthaus[1], D. Lersch[1], G. Pascovici[1], M. Seidlitz[1], B. Siebeck[1], J. Taprogge[1,3], N. Warr[1], A. Wiens[1], O. Zell[1]

[1] Institut für Kernphysik, Universität zu Köln, Zülpicher Straße 77, 50937 Köln, Germany
[2] Department of Physics, Lund University, 22100 Lund, Sweden
[3] Instituto de Estructura de la Materia CSIC, 28006 Madrid, Spain

Received: 5 June 2019 / Accepted: 22 November 2019 / Published online: 24 January 2020

Communicated by A. Jokinen

Abstract Several experiments were conducted at the 10 MV Van-de-Graaff tandem accelerator at the Institute of Nuclear Physics, Cologne, to detect proton emission from the isomeric 6457-keV 10^+ state in ^{54}Ni. Excitation functions for two fusion–evaporation reactions were measured to maximise the population of the rare two-neutron evaporation channel from a ^{56}Ni compound nucleus. The search for delayed proton emission was based on the ^{28}Si(^{28}Si, $2n$)^{54}Ni reaction at a beam energy of 70 MeV. For this reaction, a cross-section limit for the population of the 10^+ state in ^{54}Ni and its proton-decay branch was determined to be $\sigma < 22$ nb.

1 Introduction

Theoretical predictions for proton radioactivity were made by Goldansky for isotopes at the proton drip line in 1960 [1]. First decay by proton emission was discovered one decade later. Protons were emitted from a high-spin isomeric state in ^{53}Co, located at an excitation energy of 3.2 MeV [2,3]. Ground-state proton radioactivity was discovered 12 years later for the nucleus ^{151}Lu in an experiment using the velocity filter SHIP at GSI [4]. After these discoveries more than 40 proton-emitting states (from ^{108}I [5] to ^{185}Bi), including emission from long-lived isomeric states, have been established experimentally. A recent review summarises these achievements [6]. Of special interest are the three lightest proton emitters: ^{53m}Co [2,3], ^{54m}Ni [7], and ^{94m}Ag [8], which all represent high-spin and high-excitation isomers built on an aligned multi-hole configuration of the wave function relative to the doubly-magic nuclei ^{56}Ni and ^{100}Sn, respectively.

The excitation scheme of ^{54}Ni was found to comprise an isomeric 10^+ state at 6457 keV with a half-life of $T_{1/2} = 152(4)$ ns. This is displayed in Fig. 1. The isomer was identified in an experiment conducted at the GSI fragment separator together with the RISING stopped-beam Ge-detector array [7]. The isomeric 10^+ state in ^{54}Ni is the isobaric analog of the 6527 keV 10^+ isomer in ^{54}Fe [9].

Besides these findings the measurement also showed convincing evidence for a discrete $\ell = 5$ proton-decay branch into the first excited $9/2^-$ state of the daughter nucleus ^{53}Co [7]. A delayed γ-ray transition of 1327 keV was observed, which could not be assigned to ^{54}Ni or neighbouring Ni isotopes. However, a conclusive explanation of this transition is the known 1327-keV γ-ray transition from the first excited $9/2^-$ state into the $7/2^-$ ground state in ^{53}Co. The $9/2^-$ state in ^{53}Co is populated via a proton-decay branch from the isomeric 10^+ state of ^{54}Ni. Next to the proton emission with an energy of 1.22 MeV into the $9/2^-$ state, an alternative decay branch may exist populating directly the $7/2^-$ ground state of ^{53}Co. In this case a proton with an energy of 2.55 MeV is expected to be emitted with an angular momentum of $\ell = 7$. The proton-decay energies are based on a recent mass measurement of the ground state of ^{54}Ni [10].

The early RISING experiments did not include particle detectors at the FRS focal plane where the isomers were collected and identified via their consecutive γ-ray decays. Direct detection of proton emission was not foreseen. Moreover, the direct detection of the proton-decay branch with relativistic fragments is extremely challenging even with an improved experimental setup. For instance, using an active silicon detector as stopper, the incoming Ni isotopes deposit several GeV at the position of the Bragg peak. Due to the isomeric half-life of only $T_{1/2} = 152(4)$ ns it is necessary to detect and disentangle simultaneously a tiny signal from the

[a] e-mail: preiter@ikp.uni-koeln.de

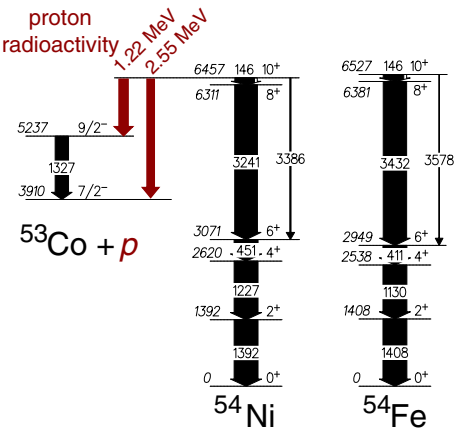

Fig. 1 Decay scheme for ^{54}Ni including the anticipated (1.22 MeV) and expected (2.55 MeV) proton emission from the 10^+ isomer in ^{54}Ni into the $9/2^-$ and $7/2^-$ daughter states in ^{53}Co, respectively. Data are taken from Ref. [7] with proton-decay energies adjusted for a recent ^{54}Ni mass measurement [10]

isomeric protons with energies of 1.22 MeV or 2.55 MeV sitting on top of the huge GeV signal during the rise time or at the saturation level of the large pulse from the implanted ^{54}Ni fragments. This is a severe challenge even when applying contemporary sampling-ADC techniques.

The difficulty to identify the low-energy protons after fragmentation reactions motivated an independent experiment. Different from the GSI experiment, the new measurement was based on a fusion–evaporation reaction forming ^{56}Ni as a compound nucleus. This approach allowed for favourable, near background free conditions for the detection of delayed proton emission. However, for this measurement the cross-section to populate the neutron-deficient residue ^{54}Ni via the two-neutron evaporation channel from ^{56}Ni was expected to be at best in the few μb regime [11]. In particular the population of the 10^+ isomer at 6.5-MeV excitation energy in ^{54}Ni was challenging due to the low proton binding energies during the evaporation cooling of the neutron-deficient ^{56}Ni compound nucleus. Moreover, this unknown isomeric ratio for populating the isomeric 10^+ state determined directly the observable proton yield from the interesting decay branch.

The first part of the paper describes excitation-function measurements with two different reactions. They were investigated to optimise the population of the high-spin and high excitation-energy isomer. A dedicated experiment to search for delayed proton emission from ^{54}Ni is described in the second part of this paper, followed by a brief summary.

2 Experimental procedure

The experiment was set up at the 10 MV FN Van-der-Graaff tandem accelerator at the Institute of Nuclear Physics at the University of Cologne. A schematic drawing of the experimental setup is shown in Fig. 2. It is based on two vacuum chambers; in the first 'target chamber', the heavy-ion beam interacted with the target nuclei and compound nucleus formation occurred. Several high-purity germanium (HPGe) detectors and a neutron-detector array, consisting of five NORDBALL detectors [12] surrounded the target chamber. These γ-ray and neutron detectors were used to identify the different reaction channels and to enrich the rare two-neutron evaporation channel in the data stream by requiring prompt γ-ray and neutron hardware coincidences.

Due to the half-life of $T_{1/2} = 152(4)$ ns of the 10^+ state of ^{54}Ni and due to the velocity of the recoiling nuclei of sev-

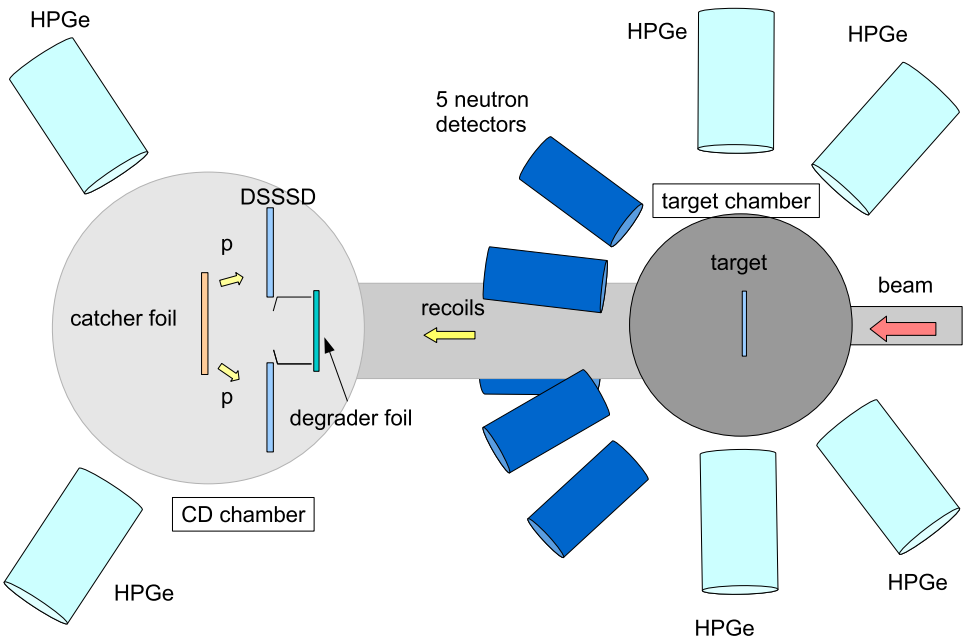

Fig. 2 Setup of the ^{54}Ni experiment (not to scale). The beam enters from the right and interacts with the thin target foil situated in the first vacuum chamber. The recoiling reaction products move in a narrow cone forward along the beam axis. In the second chamber the nuclei are decelerated by a degrader foil and are implanted into the catcher foil which is sitting close to a CD-shaped DSSSD. Emitted protons can be detected in the DSSSD at backward angles with respect to the beam direction. See text for further details

Table 1 Characteristics of γ-ray transitions used to determine the relative yields of evaporation channels for different beam energies. γ-ray energies are taken from Ref. [14]

Isotope	γ-ray energy (keV)	Transition ($I_i \rightarrow I_f$)	Evaporation channel
^{53}Fe	1328.2(3)	$9/2^- \rightarrow 7/2^-$	$2p1n$
	1011.2(2)	$11/2^- \rightarrow 9/2^-$	
^{53}Mn	1441.2(1)	$11/2^- \rightarrow 7/2^-$	$3p$
^{52}Mn	869.9(2)	$7^+ \rightarrow 6^+$	$3p1n$
^{51}Mn	237.3(2)	$7/2^- \rightarrow 5/2^-$	$1\alpha1p$
^{50}Cr	783.32(3)	$2^+ \rightarrow 0^+$	$1\alpha2p$
^{46}V	423.5(1)	$5^+ \rightarrow 3^+$	$1p1n$
^{46}Ti	889.277(3)	$2^+ \rightarrow 0^+$	$2p$
^{45}Ti	292.77(5)	$3/2^+ \rightarrow 3/2^-$	$2p1n$

eral percent of the speed of light, proton emission was predominantly *not* taking place close to the target. Thus, a second 'CD chamber' was placed 30 cm downstream the beam line. Here, the recoiling evaporation residues were stopped and collected close to an annular CD-shaped double-sided silicon-strip detector (DSSSD). On one side, the DSSSD had 32 equidistant rings covering the active area between 32-mm and 85-mm diameter. The segmentation on the other side of the DSSSD consisted of 64 sectors, giving rise to $32 \times 64 = 2048$ pixels. The recoils as well as the beam particles moved through the large physical aperture of 28-mm diameter in the center of the DSSSD. At this position clean conditions for proton spectroscopy were provided, because the DSSSD detector was protected against direct impact of scattered beam particles.

At the entrance of the DSSSD chamber the incoming beam particles and reaction products first passed a thin degrader foil. The degrader foil slowed down the recoiling evaporation residues and allowed to stop these nuclei close to the surface of a subsequent catcher foil. The high-energetic primary-beam particles passed through both foils and were finally stopped in a beam dump several meters downstream. The annular DSSSD was positioned under backward angles with respect to the beam axis and the catcher foil, where the evaporation residues were collected. Delayed proton emission (from ^{54}Ni) could thus be detected under backward angles by the DSSSD. The DSSSD chamber was surrounded by HPGe detectors for γ-ray inspection as well.

The DSSSD spectra were calibrated with a triple-α source consisting of ^{239}Pu, ^{241}Am, and ^{244}Cm, before and after the beam time. The HPGe-detector spectra were calibrated with standard ^{152}Eu and ^{226}Ra sources, before and after the beam time.

2.1 Excitation-function measurement

The isospin $T_z = -1$ nucleus ^{54}Ni is located beyond the $N = Z$ line. It is thus hardly accessible by fusion–evaporation reactions. An experiment described by Gadea *et al.* [11] detected γ-ray decays from excited states up to the spin $I^\pi = 6^+$ yrast state at an excitation energy of 3071 keV in this nucleus. The ^{24}Mg(^{32}S, 2n)^{54}Ni reaction was used. However, the isomeric 10^+ state of interest has a considerable higher excitation energy of 6457 keV, because yrast states with $I > 6$ in ^{54}Ni and its isospin mirror ^{54}Fe require particle–hole excitations across the shell gaps at particle numbers $N, Z = 28$.

The cross-section to populate this high-lying 10^+ state in ^{54}Ni via the same compound-nucleus reaction was unknown. Therefore, two series of measurements employing the fusion–evaporation reactions ^{32}S $+^{24}$ Mg and ^{28}Si $+^{28}$ Si were performed to study excitation functions. Note that both reactions produced the same compound nucleus ^{56}Ni. The yields of different evaporation residues were investigated by means of γ-ray spectroscopy.

The ^{32}S beam was delivered at four different beam energies of 82 MeV, 85 MeV, 90 MeV, and 95 MeV for the ^{32}S $+^{24}$ Mg reaction. A self-supporting ^{24}Mg target with a thickness of 0.43 mg/cm^2 was irradiated. Four HPGe detectors at the target position recorded prompt in-beam γ-ray spectra (cf. Fig. 2). Two trigger conditions were implemented: first a coincidence of at least two HPGe-detector signals, second a coincidence of at least one neutron-detector signal and one HPGe-detector signal.

The different evaporation channels were identified by the peaks from γ-ray transitions of known low-lying states of the evaporation residues. Besides the ^{32}S $+^{24}$ Mg reaction also reaction products from the fusion–evaporation channels of the ^{32}S $+^{16}$ O reaction were detected. They were caused by oxygen impurities on the surface of the Mg-target layer. Prominent γ-ray lines emitted from excited states in ^{45}Ti, ^{46}Ti, and ^{46}V nuclei were observed.

To compare the population of the different reaction channels dependent on the four different beam energies, specific γ-ray transitions and their intensities were determined. For the various reaction channels the γ-ray transitions summarised in Table 1 were used. Prompt $\gamma\gamma$-coincidence matrices were analysed to confirm the known level schemes of

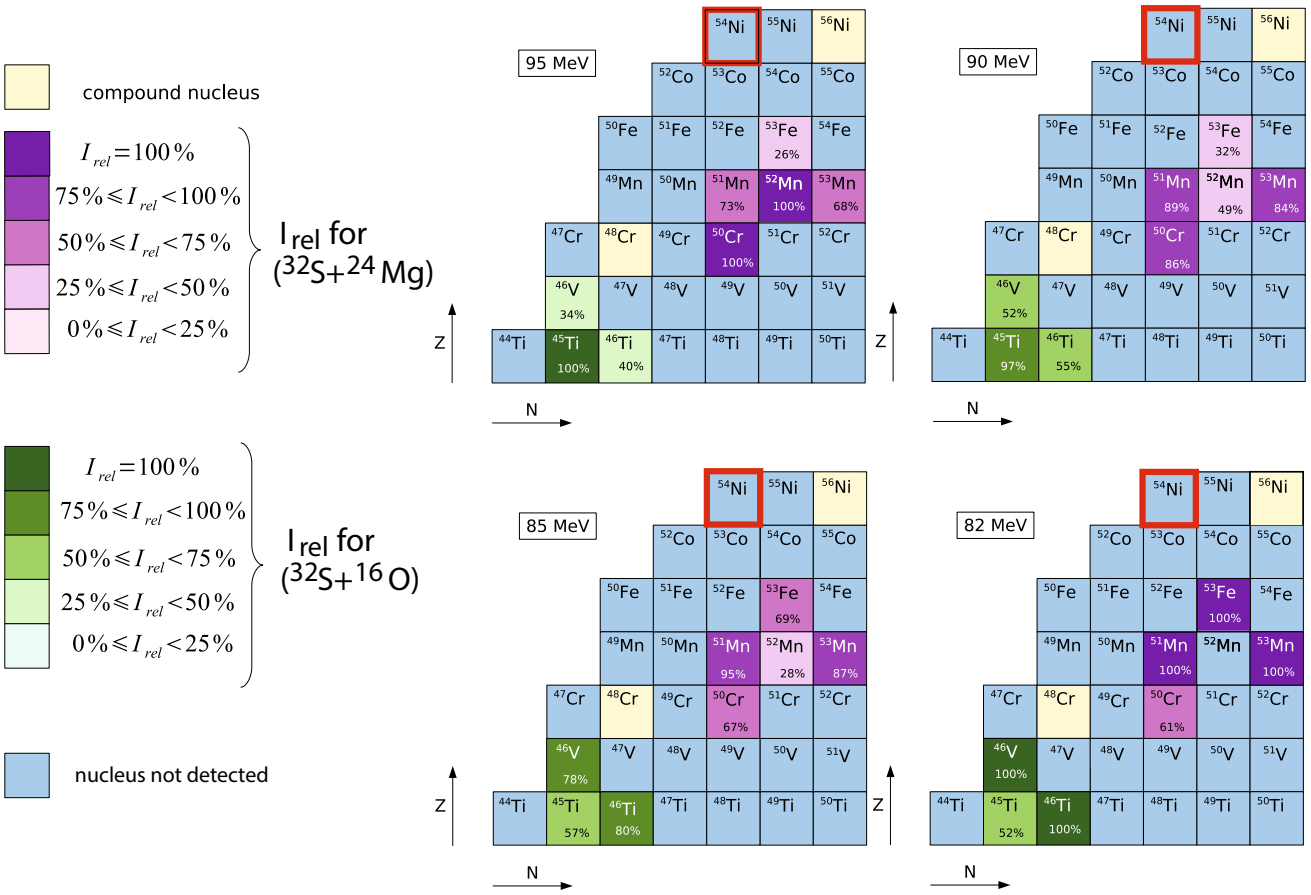

Fig. 3 Part of the table of isotopes with the identified reaction products following the fusion–evaporation reactions ^{32}S +^{24} Mg and also between beam particles and oxygen contaminants on the surface of the ^{24}Mg target layer (^{32}S+^{16}O). The colour depth is chosen with respect to the efficiency corrected yields of the γ-ray transitions listed in Table 1. For more details, see Tables 3.1, 3.2, 3.4, and 3.5 in Ref. [13]

the reaction channels ^{50}Cr, ^{51,52,53}Mn, and ^{53}Fe. The relative intensities of the prominent γ-ray lines were corrected for γ-ray detection efficiency, different beam intensities, and measuring-time periods of the four runs. The detailed numerical results can be found in Chapt. 3 of Ref. [13].

The relative intensities for the different reaction channels are displayed in Fig. 3 including the relevant part of the chart of nuclides. Marked in yellow are the two compound nuclei, ^{56}Ni for the reaction ^{32}S +^{24} Mg, and ^{48}Cr for the reaction ^{32}S +^{16} O. The observed reaction products of the fusion evaporation of the ^{32}S beam with the ^{24}Mg target are presented in shades of magenta. The products of the fusion evaporation of the beam with the oxygen contamination (^{32}S+^{16}O) are displayed in green. The colour depth is correlated to the yields of the transitions listed in Table 1. The production of lighter nuclei, like ^{50}Cr or ^{51}Mn, is increasingly favoured with increasing ^{32}S-beam energy. At lower beam energies heavier nuclei like ^{53}Fe are populated stronger. The same tendency is observed for the products of the ^{32}S +^{16} O reaction. ^{45}Ti shows an increased yield for the beam energy of 95 MeV, whereas the relative intensity of ^{46}V is smaller.

To avoid the contamination due to immediate surface oxidation of the ^{24}Mg target foil, the symmetric fusion–evaporation reaction with a ^{28}Si beam and a ^{28}Si target was investigated. For this measurement, the High-efficiency Observatory for γ-Ray Unique Spectroscopy (HORUS) array [15] at the Cologne tandem accelerator was employed to detect the emitted γ rays. HORUS consisted of 14 HPGe detectors with BGO shields and had an efficiency of 1.8% at an energy of 1332 keV. Neutron detectors were not available. Four different beam energies were probed for the ^{28}Si beam: 66 MeV, 70 MeV, 74 MeV, and 80 MeV. The thickness of the self-supporting ^{28}Si target was 0.096 mg/cm^2.

Like for the previous reaction study the relative intensities of γ-ray transitions from the dominating evaporation residue channels (see Table 1) were determined for this experiment. The results are summarised in Fig. 4 and more detailed information is available in Chapt. 3 of Ref. [13]. As expected no γ-ray lines from ^{41,42}Ca caused by reactions with oxy-

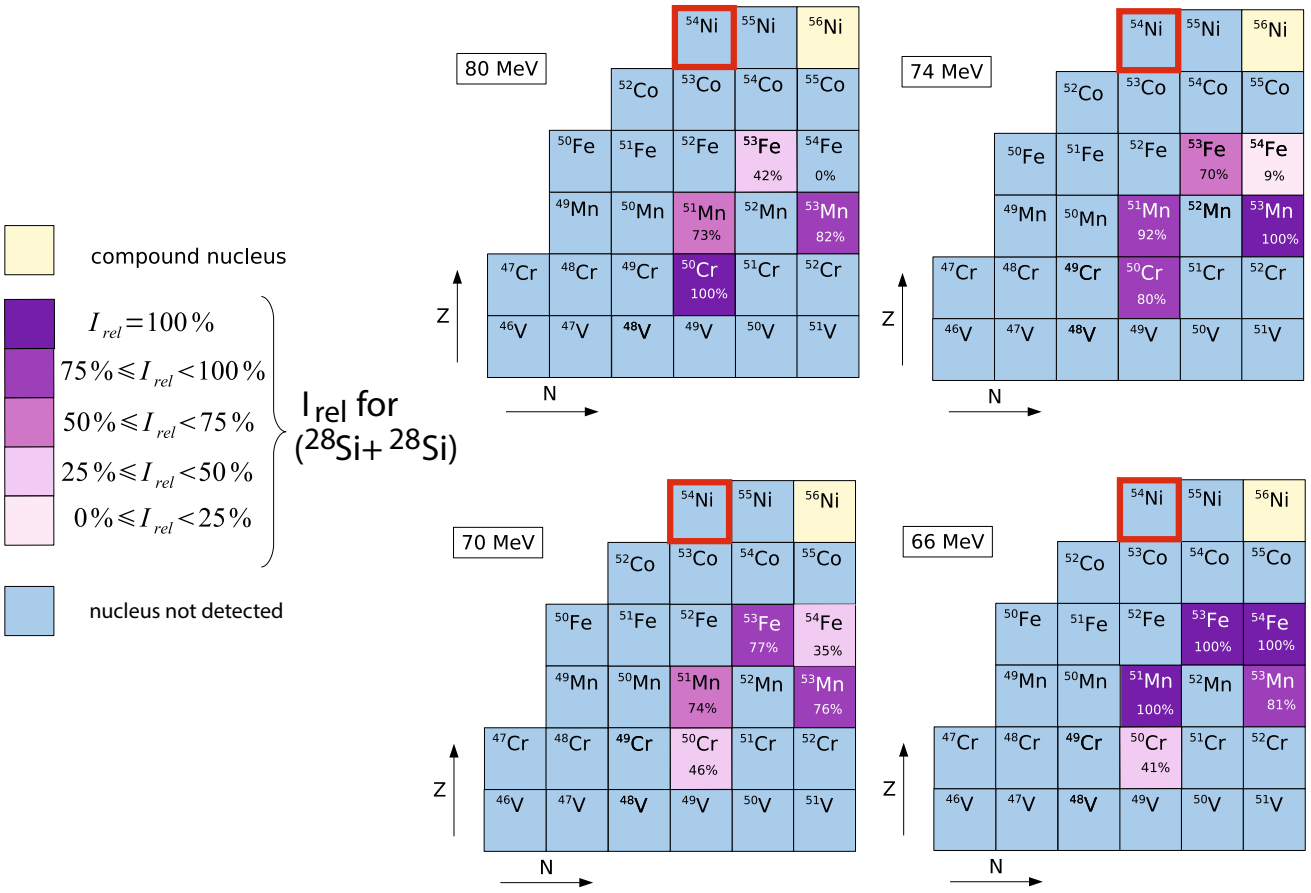

Fig. 4 Part of the table of isotopes with the products of fusion–evaporation reactions formed by the symmetric beam and target combination ^{28}Si +^{28} Si. The colour depth is chosen with respect to the yields of the transitions in Table 1

gen nuclei were observed in the spectra. In contrast to the ^{32}S +^{24} Mg experiment the two-proton evaporation channel ^{54}Fe was clearly identified via the $2^+ \rightarrow 0^+$ ground-state transition with an energy of 1408 keV [14] for the three lower beam energies with the symmetric reaction. The ^{52}Mn channel could not be identified unambiguously due to the lack of coincident neutron-evaporation detection; it was only observed in the ^{32}S +^{24} Mg experiment. Comparable results were obtained for the main reaction channels for both reactions: At the lowest beam energy of 66 MeV the population of neutron-deficient reaction channels like ^{53}Fe and even ^{54}Fe is enhanced. At higher beam energies the evaporation of more nucleons is favoured, populating lighter residues like e.g. ^{50}Cr.

Cross-section calculations for both reactions were performed with the computer codes PACE4, as part of the LISE++ package [16], and CASCADE [17]. The predictions were compared with the experimentally observed yields for the population of different residual nuclei. The comparison between calculated relative cross-sections and the experimentally observed intensities showed for the PACE4 results a discrepancy to the observations given in Figs. 3 and 4. For decreasing beam energies the PACE4 calculations predicted decreasing relative cross-sections for heavier nuclei, like ^{53}Fe and ^{53}Mn. Calculations performed with CASCADE confirmed the measured tendency that heavier reaction products show higher relative cross-sections at lower beam energies.

The predicted CASCADE cross-sections were minute for the population of ^{54}Ni via the ^{32}S +^{24} Mg reaction for all beam energies between 65 and 95 MeV. However, a small cross section of 10–20 μb was given by CASCADE for the population of ^{54}Ni via the symmetric ^{28}Si +^{28} Si reaction at beam energies between 63 and 70 MeV (see Fig. 4.1 in Ref. [13]). To account for the excitation energy of the 10^+ state of ^{54}Ni at 6.5 MeV [7] the ^{28}Si +^{28} Si reaction at a beam energy of 70 MeV was chosen for the main production experiment. Considering the separation energy that is taken away by the two neutrons, the remaining excitation energy of ^{54}Ni should be sufficient to populate states above the isomer in the range $E_{ex} = 6.5$–10.5 MeV. The symmetric ^{28}Si+^{28}Si reaction also favours the population of states at higher angular momentum which is relevant for the high spin of the isomer.

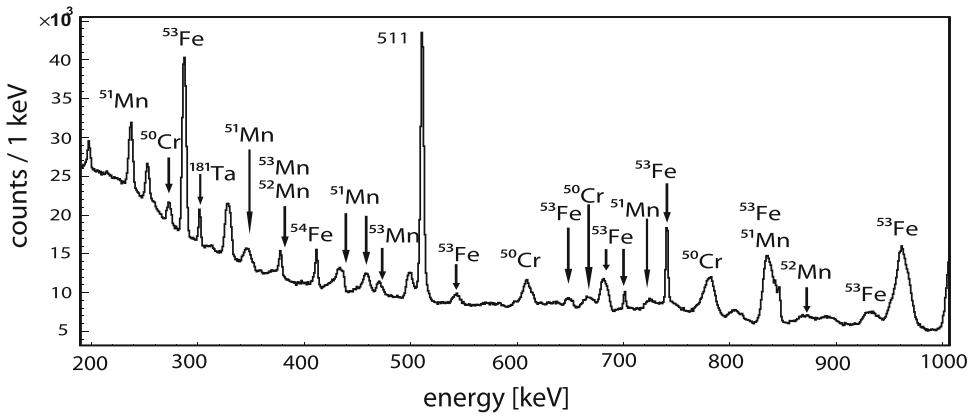

Fig. 5 Part of the Doppler-corrected in-beam γ-ray spectrum ($E_\gamma = 200$–1000 keV) measured at the target chamber for the ^{28}Si $+^{28}$ Si reaction at a beam energy of 70 MeV. Labels above γ-ray peaks indicate the identified residual nuclei as well as the background at 511 keV stemming from e^+e^- annihilation

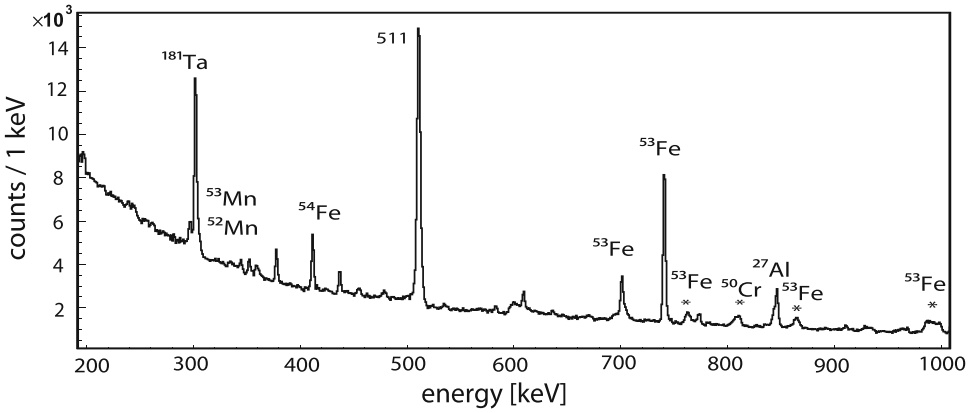

Fig. 6 Part of the γ-ray spectrum ($E_\gamma = 200$–1000 keV) at the 'CD chamber'. The spectrum is dominated by γ-ray transitions from known isomers populated in the ^{28}Si $+^{28}$ Si reaction at a beam energy of 70 MeV. The broad peaks, which are marked with asterisks ($\star$) are caused by intense γ-ray transitions from prompt events at the target position, which are Doppler shifted to higher energies and broadened due to the missing Doppler correction. Background peaks are also visible at 511 keV (e^+e^- annihilation) and 301 keV. The latter is due to Coulomb excitation of ^{181}Ta nuclei in the degrader foil hit by the primary ^{28}Si beam

3 Data analysis and experimental results

The main experiment for the direct observation of proton emission from the ^{54}Ni isomer lasted 10 days. The setup operated with a ^{28}Si beam of 70 MeV and an average beam intensity of $I = 1.4 \times 10^{10}$ ions/s. A pulsed beam was provided with a pulse length of 5 ns and a periodic time of 800 ns. The idea was to measure the proton emission of the isomeric 10^+ state with a half-life of $T_{1/2} = 152(4)$ ns in the beam pauses with low particle and γ-ray background. The beam impinged on a ^{28}Si target with a thickness of 0.33 mg/cm^2. The recoils passed the degrader foil in the CD chamber, made of 4.7 mg/cm^2 thick tantalum, with a velocity of almost $v/c = 3.7\%$. They were implanted at an estimated depth of 0.47 mg/cm^2 into the catcher foil made of aluminium. The thickness of the catcher foil was 1.2 mg/cm^2. When proton emission took place into the backward hemisphere, the protons were supposed to be re-emitted out of the catcher foil and detected by the DSSSD (cf. Fig. 2).

In a first step the γ-ray spectra of the HPGe detectors at the target chamber as well as at the CD chamber were investigated to screen the population of the reaction channels during the beam time. Figure 5 shows a part of the γ-ray spectrum with prompt events measured at the target chamber. In Fig. 6 the part of the γ-ray spectrum with the isomeric decay events detected at the CD chamber is shown. Some peaks in Fig. 6 are marked with an asterisk, which arise from prompt γ-ray emission after reactions at the target chamber and appear at too high energies in this spectrum due to their Doppler shift. Both γ-ray spectra were taken with the prompt neutron–γ trigger being active.

The γ-ray spectra at the target and CD chamber confirm the population pattern of isotopes as it is expected from the results discussed in Sect. 2. The most interesting question, however, is whether it is possible to find evidence for the population of the 10^+ isomer in ^{54}Ni, which should be implanted into the catcher foil.

If the 10^+ state de-excited by γ-ray decay to the ground state of ^{54}Ni, amongst others the 451-1227-1392-keV $6^+ \rightarrow$

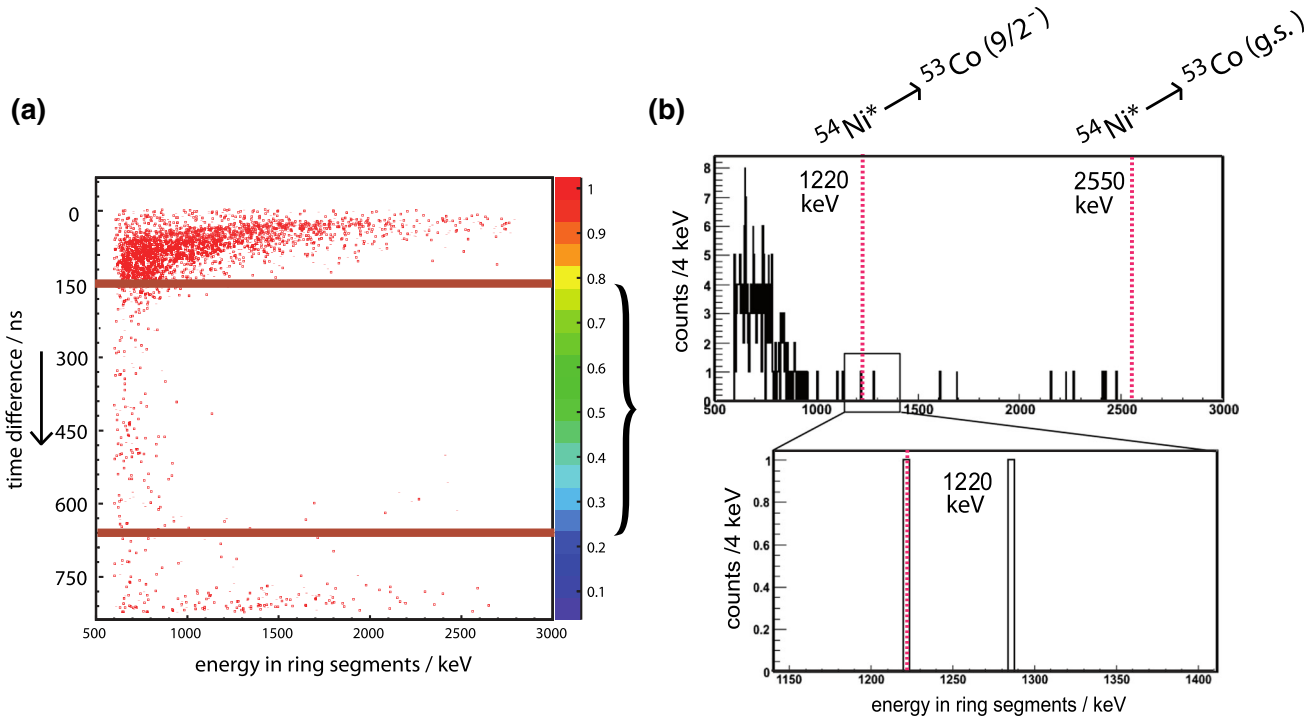

Fig. 7 **a** Time difference between trigger and beam pulse versus the energy in DSSSD-ring segments; additionally, the detection of at least one neutron is required. **b** Projection of panel (**a**) onto the x axis for the time interval $\Delta t = 150$ ns-660 ns. Dashed red lines indicate the position of expected proton-emission energies (cf. Fig. 1)

$4^+ \rightarrow 2^+ \rightarrow 0^+$ cascade of ^{54}Ni (cf. Fig. 1) should be visible in the γ-ray spectrum in Fig. 6. Unfortunately, no clear evidence of peaks at any of these energies can be identified (cf. Figs. 4.8–4.11.in Ref. [13]). If proton emission takes place, an indirect evidence of this proton emission would be the detection of the $9/2^- \rightarrow 7/2^-$ transition in ^{53}Co, as it was observed in the RISING experiment at GSI described in Ref. [7]. This transition, however, is completely masked by the 1328-keV doublet arising from the $9/2^- \rightarrow 7/2^-$ 'mirror transition' in ^{53}Fe. In fact, the 701–1011–1328-keV cascade stemming from the 3040-keV $19/2^-$ isomer in ^{53}Fe and the isomeric 741-keV $3/2^- \rightarrow 7/2^-$ decay in ^{53}Fe [14] dominate the delayed γ-ray spectrum in Fig. 6. Hence, direct evidence for the population of the 10^+ isomer in ^{54}Ni cannot be provided by the γ-ray spectrum of Fig. 6. In turn, the dominant presence of delayed γ rays from the $2p1n$ reaction channel ^{53}Fe in Fig. 6 proves that the experiment was conceptually working.

The most relevant and interesting spectra are the energy spectra from the DSSSD, where the proton emission with energies of 1.22 MeV and 2.55 MeV should be visible (cf. Fig. 1) in the case of population and proton decay of the 10^+ isomer in ^{54}Ni. Concerning the detailed treatment of particle energies, we refer to the appendix and Chapt. 4.5.2 of Ref. [13].

Time correlations in the data are highly beneficial for the investigation of isomeric events, such as the decay from the 10^+ state of ^{54}Ni. In Fig. 7a the time difference between the DSSSD trigger and the beam pulse is shown on the y axis as a function of the energy detected in the DSSSD on the x axis from all DSSSD rings. The conditions and corrections specified in the appendix and Ref. [13] were applied. The spectrum has the additional condition that at least one neutron was detected in coincidence with the DSSSD signal. In the upper part of Fig. 7a the events are related to the beam pulse itself. Between about 150 ns and 660 ns, only (isomeric) decay events are detected, prior to the next beam pulse.

The time spectrum was calibrated, considering that prompt signals were detected at $\Delta t = 0$ ns and that the TDC range of 4096 channels equated to the nominal 1.2 μs range. The DSSSD was shielded against the primary beam. Nevertheless, a relatively large number of prompt background events was measured. A possible explanation for this background are scattered beam particles or light evaporated charged particles from the target area. At about 150 ns after the beam pulse, i.e. after about one half-life of the 10^+ state of ^{54}Ni, still around half of the ^{54}Ni nuclei are supposed to be detectable. The short-lived background from the beam pulse, however, has disappeared.

Within a time range from 150 to 660 ns the particle spectrum is displayed in Fig. 7b. In this time window 45.2%

of protons emitted from the 10^+ isomer in ^{54}Ni should be located. Figure 7b shows the projection of the time spectrum onto the x axis for this time interval. The background in the DSSSD spectrum is reduced very well by four orders of magnitude in comparison with the initial DSSSD spectrum. However, neither is a peak-like structure observed in Fig. 7b at an energy of about 1.22 MeV - which would verify the proton emission into the first excited state of ^{53}Co - nor at the energy of about 2.55 MeV - which would be a hint for proton emission into the ground state of ^{53}Co. An accumulation of counts is located around 2.410 MeV, which is 140 keV away from the expected peak energy. This difference amounts more than two times the energy resolution. An inspection of the time distribution shows that all of the counts show up at longer time differences of more than 420 ns implying a long half-life, which is not consistent with the isomeric half-life of $T_{1/2} = 152(4)$ ns of the 10^+ state in ^{54}Ni.

Based on the counts in the particle spectrum shown in Fig. 7b, the upper limit of the cross-section for proton emission from the isomeric 10^+ state in ^{54}Ni into low-lying states of ^{53}Co is calculated to $\sigma(^{54}\mathrm{Ni}(10^+);\, p) \leq 8$ nb [13]. With the proton–γ branching ratio of ~ 0.5–1.0 [7], the upper limit of the cross-section for the population of the 10^+ state of ^{54}Ni is estimated to $\sigma < 22$ nb [13].

In comparison to the results of Ref. [18] the cross-sections $\sigma(^{54}\mathrm{Ni}(10^+)\mathrm{p})$ and $\sigma(^{54}\mathrm{Ni}(10^+))$ could be downscaled by a factor of roughly five. The very low cross-section limit readily explains the non-observation of delayed ^{54}Ni γ-ray lines at, for instance, 451 keV, 1227 keV, or 1392 keV in the spectrum of Fig. 6.

The cross-section for the population of ^{54}Ni for this beam energy, predicted with the computer code CASCADE, amounts to 10–12 μb. This is almost three orders of magnitude higher than the determined upper cross-section limit $\sigma(^{54}\mathrm{Ni}(10^+))$ for the isomeric 10^+ state. The computer code PACE4, which is part of Lise++ [16], predicts for the population of ^{54}Ni an even higher cross section of $\sigma = 155\,\mu$b. Hence, the difference between the experimentally determined cross-section limit for the population of the isomeric 10^+ state and the theoretically predicted cross-section for the population of ^{54}Ni is almost four orders of magnitude.

4 Conclusions

To search for proton emission from the 10^+ isomer in ^{54}Ni, a dedicated experimental setup was developed, trying to exploit the recoil-decay method to detect delayed proton radiation in either prompt or delayed coincidences with γ rays and neutrons. Two attempts with different fusion–evaporation reactions leading to the compound nucleus ^{56}Ni and thus possible population of ^{54}Ni via two-neutron evaporation were performed.

Extensive preparations and test measurements were conducted to identify the most promising choice of beam-target combination and beam energy. The production experiment worked conceptually as expected, but the fusion–evaporation cross-section to populate the 10^+ isomer of interest in ^{54}Ni was found to be too low. Thus, other combinations of production reaction and decay measurement are called for to settle the open questions of proton-decay branching ratios and associated isospin-symmetry questions posed earlier [7].

Acknowledgements Open Access funding provided by Projekt DEAL. We would like to thank the accelerator staff at the University of Cologne for the efforts to deliver heavy-ion beams of excellent quality, as well as the Swedish Research Council (contract VR 2008-4240 and VR 2016-3969) for financial support.

Data Availability Statement This manuscript has no associated data or the data will not be deposited. [Authors' comment: The data that support the findings of this study are available from the corresponding author on reasonable request.]

Appendix A

The consideration of the passive layers on the DSSSD surface is relevant for energy calibration due to different energy losses for protons and α particles. A method to correct the DSSSD energy spectra for the energy loss of the particles in the passive layers was first developed in the work of Wendt [18]. The strip detector has passive layers of SiO_2 and Al in which the incident particles lose part of their energy. First the energy loss of the α particles from the calibration source has to be calculated - depending on the detection angle of the rings the energy loss varies between 140 and 220 keV. This correction is determined with the help of the Bethe–Bloch formula, which provides a $1/E$-dependency for the energy loss of non-relativistic charged particles. Because the range of the α energies between 5155 and 5805 keV is rather small a linear fit as correction function for the recalibrated energy E_R depending on the measured energy E_M is sufficient:

$$E_R(E_M) = a_\alpha \cdot E_M + b_\alpha. \quad (1)$$

In a next step the energy loss of protons (first in the catcher foil, from where they are emitted, second in the DSSSD) has to be accounted for. For seven different assumed proton ener-

gies between 0.5 and 6.0 MeV the energy loss is calculated with the Bethe–Bloch formula depending on the angle. The original energy of the proton, E_i, is then determined with the following fit function:

$$E_i(E_M) = a_p + (E_M + d_p) + b_p + \frac{c_p}{(E_M + d_p)}. \quad (2)$$

The energy loss for the protons by these effects ranges from 110 to 170 keV.

With the six parameters a_α, b_α, a_p, b_p, c_p, and d_p established, the initial energy for every measured particle can be calculated assuming that this particle is a proton:

$$E_i(E_M) = a_p + (E_R(E_M) + d_p) + b_p + \frac{c_p}{(E_R(E_M) + d_p)}. \quad (3)$$

When an emitted proton hits the 300 μm thick DSSSD the signal should also be detectable at the backside of the detector. One condition for a proper particle event is thus that the multiplicity of events in the rings and segments are both equal one. Moreover, the energy difference of the measured signal is required to be less than 200 keV. Furthermore, the intrinsic energy resolution for an event of 1.22 MeV is extrapolated from the α-particle calibration to be approximately 40 keV (FWHM).

The distance between the target and catcher foils is based on the calculated angular distribution of the evaporation residues. The hole inside the DSSSD and the opening angle of the catcher foil allows a homogeneous irradiation. Consequently, the extended source size causes a broadening of the energy peaks which was calculated to be approx. 32 keV and thus comparable with the expected energy resolution for protons at 1.22 MeV. A third effect, which is included as contribution to the width of the energy peak, are differences in energy loss for the beam and residue in the target and the difference in implantation depth. For protons of 2.55 MeV the impact of the extended source size is only around 13 keV, while the final energy resolution is calculated to be around 58 keV. The details of the calibration and expected peak width are given in Ref. [18].

References

1. V.I. Goldansky, Nucl. Phys. A **19**, 482 (1960)
2. J. Cerny, J. Esterl, R.A. Gough, R.G. Sextro, Phys. Lett. B **33**, 284 (1970)
3. K.P. Jackson, C.U. Cardinal, H.C. Evans, L.A. Jelley, J. Cerny, Phys. Lett. B **33**, 281 (1970)
4. S. Hofmann, W. Reisdorf, G. Münzenberg, F.P. Hessberger, J.R.H. Schneider, P. Armbruster, Z. Phys. A **305**, 111 (1982)
5. K. Auranen et al., Phys. Lett. B **792**, 187 (2019)
6. M. Pfützner, M. Karny, L.V. Grigorenko, K. Riisager, Rev. Mod. Phys. **84**, 567 (2012)
7. D. Rudolph et al., Phys. Rev. C **78**, 021301(R) (2008)
8. I. Mukha et al., Phys. Rev. Lett. **95**, 022501 (2005)
9. Yang Dong, Hua Junde, Nucl. Data Sheets **121**, 1 (2014)
10. P. Zhang et al., Phys. Lett. B **767**, 20 (2017)
11. A. Gadea et al., Phys. Rev. Lett. **97**, 152501 (2006)
12. S.E. Arnell et al., Nucl. Instr. Meth. A **300**, 303 (1991)
13. K. Geibel, PhD thesis, University of Cologne, ISBN 978-3-8439-0660-9 (2012). https://www.ikp.uni-koeln.de/fileadmin/data/reiter/theses/geibel_diss.pdf
14. ENSDF database. http://www.nndc.bnl.gov/ensdf
15. A. Linnemann, PhD thesis, University of Cologne (2005)
16. D. Bazin, O.B. Tarasov, M. Lewitowicz, O. Sorlin, Nucl. Instr. Meth. A **482**, 307 (2002)
17. F. Pühlhofer, Nucl. Phys. A **280**, 267 (1977)
18. A. Wendt, Diploma thesis, University of Cologne (2008). https://www.ikp.uni-koeln.de/fileadmin/data/reiter/theses/wendt_diplom.pdf